Water Air Soil Pollut (2016) 227: 284
DOI 10.1007/s11270-016-2995-8

Selective Photocatalytic Degradation of Organic Pollutants Using a Water-Insoluble Zn–Schiff Base Complex

Tirusew Araya · Song Quan · Jia Man-ke · Ma Wan-hong · David Johnson · Huang Ying-ping

Received: 3 May 2016 / Accepted: 18 July 2016 / Published online: 27 July 2016
© Springer International Publishing Switzerland 2016

Abstract In this study, a novel water-insoluble zinc–Schiff base complex, Zn(II)-*N*-salicylaldehyde-2-hydroxyanil (abbreviated as Zn-salen), was synthesized and used as a heterogeneous photocatalyst for the activation of molecular oxygen to degrade organic pollutants in aqueous solution under visible light irradiation ($\lambda \geq 420$ nm). The catalyst was characterized by FT-IR, UV–vis spectroscopy, NMR, and MS analysis. Zn-salen displays a selective adsorption and degradation of electropositive organics, such as rhodamine B (RhB), methylene blue (MB), and *o*-phenylenediamine (OPD). After using cetyl trimethyl ammonium bromide (CTAB) to change sulforhodamine B (SRB) into RhB-like electropositive molecule, the degradation of SRB increased up to 96 % after 4 h of irradiation, indicating that the selectivity arises from the charge interaction between the catalyst and substrates. Zeta potential of Zn-salen also reveals that the catalyst surface is negatively charged in neutral solution, suggesting that the catalyst is selective towards positively charged substrates due to an electrostatic force of attraction. The photocatalyst was active within a wide pH range (pH 3–11) and chemically stable and can be reused over 10 times. In addition, $^1O_2$ and $O_2{\cdot}^-$ were involved in photocatalytic degradation but $O_2{\cdot}^-$ appears to be the primary reactive oxygen species.

Keywords Photodegradation · Schiff base · Selectivity · Superoxide radical

Electronic supplementary material The online version of this article (doi:10.1007/s11270-016-2995-8) contains supplementary material, which is available to authorized users.

T. Araya · H. Ying-ping
College of Hydraulic and Environmental Engineering, China Three Gorges University, Yichang 443002, China

T. Araya
e-mail: tirusew@ctgu.edu.cn

T. Araya · S. Quan · J. Man-ke · H. Ying-ping
Innovation Center for Geo-Hazards and Eco-Environment in Three Gorges Area, Yichang, Hubei Province 443002, China

S. Quan
e-mail: songquan87@126.com

J. Man-ke
e-mail: jiamanke@yeah.net

T. Araya · S. Quan · J. Man-ke · M. Wan-hong · D. Johnson · H. Ying-ping (✉)
Engineering Research Center of Eco-environment in Three Gorges Reservoir Region, Ministry of Education, China Three Gorges University, Yichang 443002, China
e-mail: chem_ctgu@126.com

M. Wan-hong
e-mail: whma@iccas.ac.cn

D. Johnson
e-mail: davjohn2602@yahoo.com

1 Introduction

Effective and low-cost oxidative removal of deleterious organic pollutants from water have been one of the major challenges in environmental remediation (Mahamuni and Adewuyi 2010; Ahmed et al. 2011).

Semiconductors based on metal oxides such as TiO_2, and Fenton or photo-Fenton process is well known as an effective advanced oxidation process (AOP) for the treatment of toxic or persistent organic pollutants (POPs) in wastewater (O'Shea and Dionysiou 2012; Kubacka et al. 2012; Chen et al. 2011a, b; Tianyuan et al. 2013; Xiaopeng et al. 2015; Boukha et al 2016). Zuo et al. also demonstrated effective photodegradation of pollutants using transition metal complex (Zuo and Deng 1997; Chen et al. 2013). In these treatment methods, hydroxyl radicals (·OH) and other reactive oxygen species (ROS) are produced and attack pollutant molecules unselectively (Liu et al. 2011). However, AOPs require UV activation and acidic conditions (pH ≤3) (Gonzalez-Olmos et al. 2012; Drozd et al. 2012) and they lack selectivity. Recently, organic transition metal complexes (TMCs), activated by visible light, have attracted attention in the search for effective and low-cost oxidative elimination of POPs (Chen et al. 2011a, b; Zou et al. 2012). Several biocompatible organic TMCs with varying combinations of metals and organic constituents have shown high photocatalytic activity at neutral pH by using H_2O_2 or molecular O_2 as the ROS source.

Metal–Schiff base complexes, a structural analogue of metalloporphyrins, are an interesting class of organic TMCs for directing electron transfer in photosynthesis (Qianqian et al. 2016). Due to the relative ease of synthesis, metal–Schiff base complexes have received much attention in the area of catalysis, luminescence, and magnetism (Vijayaraj et al. 2011; Ardo et al. 2011). The electronic character and steric effects of metal–Schiff base complexes can be modified precisely by changing the structure of ligand or introducing an additional substituent to improve their selectivity. Schiff base complexes of transition metal ions such as iron, copper, and manganese show high photocatalytic activity in degrading organic compounds (Wu et al. 2012; Liu et al. 2012). Among the organic TMC photocatalysts used for oxidative decomposition, zinc complexes had shown to be effective in degrading many organic compounds because of singlet oxygen ($^1O_2$) and the superoxide anion radical ($O_2{\cdot}^-$) produced during photo irradiation (Silva et al. 2012; Fatemeh and Kamran 2016). Due to the ease of preparation, high photosensitivity, chemical stability, and non-toxicity, zinc–Schiff base complexes draw a great attention of the research community (Liu et al. 2012; Gupta et al. 2009).

Most organic TMCs are soluble in water and employed as a homogeneous photocatalyst (Su et al. 2009) or immobilized on supports such as resin, silica, and zeolite by ion exchange, adsorption, or encapsulation (Sharma et al. 2012; Meng et al. 2011) to facilitate ease of separation. It has been reported that photocatalytic degradation efficiency can be improved by hydrophobic modification of TiO_2 surface, attributed primarily to an increased adsorption (Huang et al. 2003, 2004). Previously, it was reported that water-insoluble Schiff base complexes of copper and iron could be used directly as heterogeneous photocatalysts (Song et al. 2013, 2015) due to their high stability in the hydrophobic micro-environment (Hu et al. 2009; Cotanda et al. 2012; Buddhadeb et al. 2007).

Selectivity is one of the most desirable properties of a catalyst for the degradation of target pollutants in the presence of other components, and recently, it spurred researchers to focus in developing a selective photocatalyst. Selective degradation of pollutants can be achieved by adjusting light intensity, initial concentration of pollutants and pH of the solution (Chen et al. 2013), bandgap of the catalyst (Niu et al. 2014), and pore size and surface charge of the catalyst (Warren et al. 2014; Zhao et al. 2013). Selective adsorption of pollutants with charged polarity is mainly determined by the size and charge of the exposed surface of the catalyst, suggesting that columbic interactions are crucial in the photodegradation of pollutants (Sofianou et al. 2013; Tseng and Lin 2014). Ye et al. (2011) used fluoropolymer poly-vinylidene–fluoride-modified TiO_2 to achieve tunable photocatalytic selectivity. Similarly, titanium dioxide–graphene composite and polyoxometalate-based metal–organic framework show charge-based selectivity which is attributed to the synergistic effect of the unique pore morphology and the surface properties of the composite (Bozell et al. 1995). Cationic dyes were photodegraded selectively due to the negative surface charge of the catalyst (Zhao et al. 2014; Ali and Sandhya 2016). Generally, selectivity can be attributed to oxidation ability of certain reactive species, components, and structure of catalysts which may affect adsorption properties (Ryo et al. 2015; Wang et al. 2015; Fang et al. 2011).

Herein, a novel water-insoluble zinc–Schiff base complex, Zn(II)-*N*-salicylaldehyde-2-hydroxyanil (abbreviated as Zn-salen), was synthesized and used as a heterogeneous photocatalyst. The photocatalytic properties and photocatalytic mechanism of pollutants over

Zn-salen photocatalyst at neutral pH under visible light irradiation ($\lambda \geq 420$ nm) are discussed in detail. The response of the catalyst to the photocatalytic degradation of dyes in the presence of cationic (cetyl trimethyl ammonium bromide, CTAB) and anionic (sodium dodecyl sulfate, SDS) surfactants was also investigated to further understand the selective degradation of pollutants over the catalyst surface.

2 Experimental

2.1 Materials and Reagents

Salicylaldehyde, 2-hydroxyaniline, zinc acetate, *tert*-butanol, *p*-benzoquinone, anhydrous ethanol, and anhydrous methanol were AR grade and obtained from the Tianli Chemical Factory (Tianjin, China); rhodamine B (RhB), sulforhodamine B (SRB), methylene blue (MB), orange II (acid orange 7, Org II), benzene-1,2-diamine (*o*-phenylenediamine, OPD), and salicylic acid (SA) were purchased from the Beijing Ouhe Chemical Factory (China); 5,5-dimethyl-1-pyrroline-*N*-oxide (DMPO), 2,2,6,6-tetramethylpiperidine (TEMP), SDS, and CTAB were purchased from Sigma-Aldrich. Other chemicals were of reagent grade and used without further purification. Deionized and doubly distilled water was used throughout the investigation.

2.2 Synthesis of *N*-salicylaldehyde-2-hydroxyanil

The Schiff base ligand, salicylaldehyde-2-hydroxyanil (salen), was prepared as previously described (O'Shea and Dionysiou 2012). Salicylaldehyde (2.44 g, 0.02 mol) was added dropwise into anhydrous ethanol solution (50 mL) with 2-hydroxyaniline (2.18 g, 0.02 mmol) and refluxed at 80 °C with stirring for 4 h. The product was then separated by filtration, and the crude residue was purified three times by recrystallization in CH_3OH. Yield was 86 %; mp was ~188–190 °C; ^{1}H NMR (400 MHz, 293 K, DMSO-d_6): δ was 6.857~7.622 (m, 8H, $H_{aromatic}$), 8.965 (s, 1H, CH), 9.7555 (s, 1H, OH), and 13.811 (s, 1H, OH). ^{13}C NMR (400 MHz, 294 K, DMSO-d_6): δ was 116.52, 116.70, 118.74, 119.51, 119.60, 128.08, 132.33, 132.84, and 134.94, (s, $C_{aromatic}$); 151.14 and 160.74 (s, CO); and 161.70 (s, CN). MS (m/z) = 214.2 $[M]^+$.

Zn-salen was obtained by mixing zinc acetate and salen (1:1 molar ratio) in anhydrous ethanol. The mixture was refluxed at 80 °C for 4 h and cooled. The product was filtered, washed thoroughly with anhydrous methanol, and dried in an infrared rapid desiccator. Yield = 75 %; MS (m/z) = 338.2 $[M]^+$. The structures and synthesis of salen and Zn-salen are shown in Scheme 1.

2.3 Adsorption Experiments

The adsorption experiment was carried out in 100-mL conical flasks containing 50 mL suspension of different substrates (0.48–9.6 mg/L) and Zn-salen (0.1 g/L). These flasks were stirred on an orbital shaker at 30 °C. The concentration of RhB adsorbed on the Zn-salen surface at equilibrium was calculated as follows:

$$Q_{eq}^{-1} = \left(Q_{max} K\ C_{eq}\right)^{-1} + Q_{max}^{-1} \quad (1)$$

where Q_{eq} is the adsorption equilibrium capacity (mg/g), C_{eq} is the equilibrium concentration of solution (mg/L), Q_{max} is the saturation capacity (mg/g), and K is the equilibrium constant.

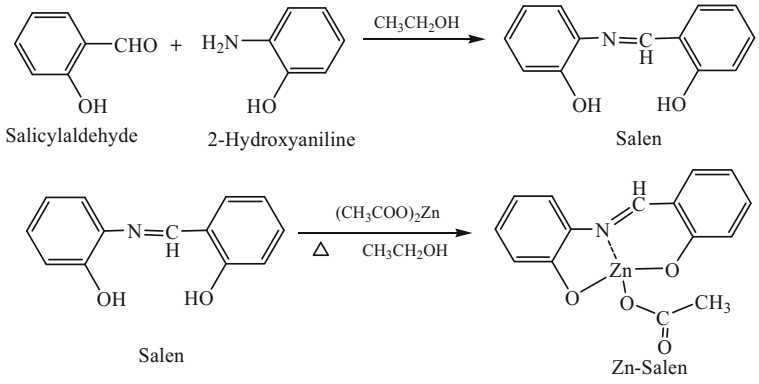

Scheme 1 Synthesis and structures of salen and Zn-salen

2.4 Photocatalytic Degradation of Substrate

The dosing level of Zn-salen was 0.1 g/L, and the initial concentration of dyes and colorless substrates were 1.0×10^{-5} and 5.0×10^{-5} mol/L, respectively. The light source was a 500-W halogen lamp positioned in a XPA series (Xujiang Mechanical and Electrical Factory, Nanjing, China) photochemical reaction chamber. A cutoff filter ($\lambda < 420$ nm) was placed outside the Pyrex jacket to ensure illumination by visible light only. The reaction mixture was then transferred to a cylindrical glass bottle, and the solution pH was adjusted. To investigate wavelength dependency, a 450-W Xenon lamp (Oriel) combined with a 10-cm IR water filter and a series of single-wavelength cutoff filters ($\lambda = 365$, 420, and 450 nm) was used as a light source.

Prior to photocatalytic degradation of the substrates, adsorption/desorption equilibrium was established by stirring the solution for 1 h in the dark. To monitor degradation progress, samples were collected at specified time intervals into an Ep tube. All the samples were centrifuged, and the concentration of dyes was monitored by full scan UV–vis spectrophotometry, while the colorless organics were analyzed with a HPLC system equipped with a Diamonsil C18 column (250 × 4.6 mm) and a UV detector at 278 nm. In the detection of SA, the optimized mobile phase consisted of 45 % methanol and 55 % phosphate solution (KH_2PO_4, pH = 3.5) and the flow rate was set at 0.5 mL/min. Thirty-five percent methanol and 65 % aqueous solution of ammonium acetate (0.01 mol/L) were used as a mobile phase for the analysis of OPD. The column temperature was maintained at 30 °C. The supernatant liquid of the photodegraded samples was monitored by a Nicolet iS50 Fourier transform infrared spectrometer. UV–vis diffuse reflectance spectra (UV–vis DRS) were obtained by a UV–vis spectrophotometer (Varian Cary 500) with $BaSO_4$ as a reflectance standard.

2.5 Determination of Hydrogen Peroxide and Active Species

Electron spin resonance (ESR) investigation was carried out on a Bruker model EPR 300E spectrometer (Bruker, Germany), which was equipped with a Quanta-Ray Nd:YAG laser (532 nm). DMSO and TEMPO were used as spin-trapping reagents to detect superoxide anion radical ($O_2^{\cdot -}$) and singlet oxygen ($^1O_2$), respectively. Measurement conditions were adjusted as follows: center field 3486.7 G, sweep width 100 G, microwave frequency 9.82 GHz, and power 5.05 mW. To minimize experimental errors, the same quartz capillary tube was used for the ESR measurements. All of the measurements were carried out at room temperature.

3 Results and Discussion

3.1 Characterization of Salen and Zn-Salen

Comparing the IR spectra of salen and Zn-salen provides information on metal–ligand bonding, as shown in Table 1. The assignments are based on typical group frequencies. The absorption bands at 2500–3046 and 1141 cm^{-1} in the IR spectrum of salen were assigned to ν(O–H) stretching and δ(O–H) rocking, respectively, indicating the existence of a phenolic hydroxyl group. These bands disappeared when Zn-salen was scanned, since Zn^{2+} replaces proton coordination to oxygen. The strong absorption band at 1631 cm^{-1} in the spectrum of Zn-salen is attributed to the coordination of the nitrogen atom of the azomethine (C=N) group to the metal ion (El-Medani et al. 2005). In addition, the IR spectrum of Zn-salen shows appreciable shifts in the ν(C–N) and ν(C–O) bands. Two bands at 746 and 514 cm^{-1} present in the spectrum of Zn-salen are assigned to ν(Zn–O) and ν(Zn–N), respectively. The salen ligand coordinates to zinc through two phenolic oxygen and an azomethine nitrogen acting as a bidentate ligand.

Table 1 FT-IR data for salen and Zn-salen

	ν(O–H) cm^{-1}	ν(C=N)	ν(C–N)	ν(C–O)	ν(Zn–O)	ν(Zn–N)
Salen	3046	1631	1306	1276, 1243	–	–
Zn-salen	–	1614	1298	1265, 1222	746	514

The UV–vis absorption spectra of salen and Zn-salen in CH_3OH are compared as shown in the online resource (Fig. S1). There are three absorption peaks at 210, 254, and 310 nm in the spectrum of salen. The peak at 250–290 nm was assigned to the π–π* transition associated with the benzenoid bond. In the UV–vis spectrum of Zn-salen, all three bands display a red shift with respect to analogous peaks in the spectrum of free salen, due to metal conjugation. In particular, the absorption at 310 nm, due to the n–π* transitions of the HC–N system between phenyl rings in salen, undergoes an intensive shift to approximately 420 nm (Claudio et al. 2001). The sizeable red shift of Zn-salen absorption, compared to the ligand, is attributed to participation of the free electron pair on the N atom of C=N in metal coordination and also the replacement of H atom of –OH by the metal ion. The coordination changes the electronic properties of the molecule, increasing visible light absorption and enhancing photocatalytic degradation.

The room-temperature DRS of Zn-salen displayed in Fig. 1 demonstrate visible light ($\lambda \leq 500$) harvesting the ability of the catalyst. The DRS display a broad absorption with an absorption edge of 520 nm, indicating that Zn-salen can efficiently utilize visible light to drive photocatalytic degradation of pollutants. According to the relationship of $(\alpha h\nu)^{1/2}$ versus the photon energy ($h\nu$), the bandgap of Zn-salen was calculated as 2.4 eV as shown in the inset of Fig. 1b.

Zn-salen is a bidentate metal–Schiff base with zinc(II) as the metal core and the salen as the ligand. The scanning electron microscope (SEM) images of Zn-salen in Fig. 2 show a dominant rod-like structure indicating a uniform crystallization. The rod-like structures of Zn-salen were several micrometers long and 1–3 μm wide and sparsely entangled.

3.2 Adsorption of Target Organic Compounds by Zn-Salen

Adsorption of substrates on the catalyst surface affects degradation efficiency. The adsorption capacity of Zn-salen for azo dyes at 25 °C was characterized using a Langmuir isotherm. Substrates with different charge distributions were used to study the adsorption behavior of Zn-salen. The adsorption capacities of Zn-salen for different substrates are displayed in Table 2. The adsorption capacities of RhB ($Q_{max} = 0.023$ mg/g, $k = 2.01 \times 10^3$) and MB ($Q_{max} = 0.025$ mg/g, $k = 1.13 \times 10^3$) are much higher than those of SRB ($Q_{max} = 0.002$ mg/g, $k = 3.46 \times 10^2$) and Org II ($Q_{max} = 0.004$ mg/g, $k = 6.78 \times 10^2$). Even though all substrates can be surface adsorbed due to hydrophobic

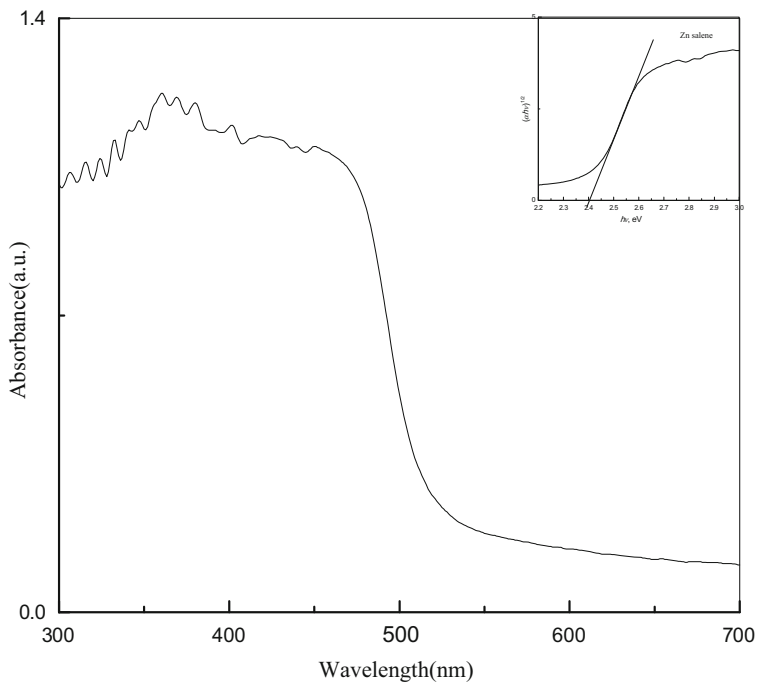

Fig. 1 UV–vis diffuse absorption spectra of Zn-salen with the *inset* of the optical bandgap obtained from the plots of $(\alpha h\nu)^{1/2}$ versus the photon energy ($h\nu$) of the Zn-salen

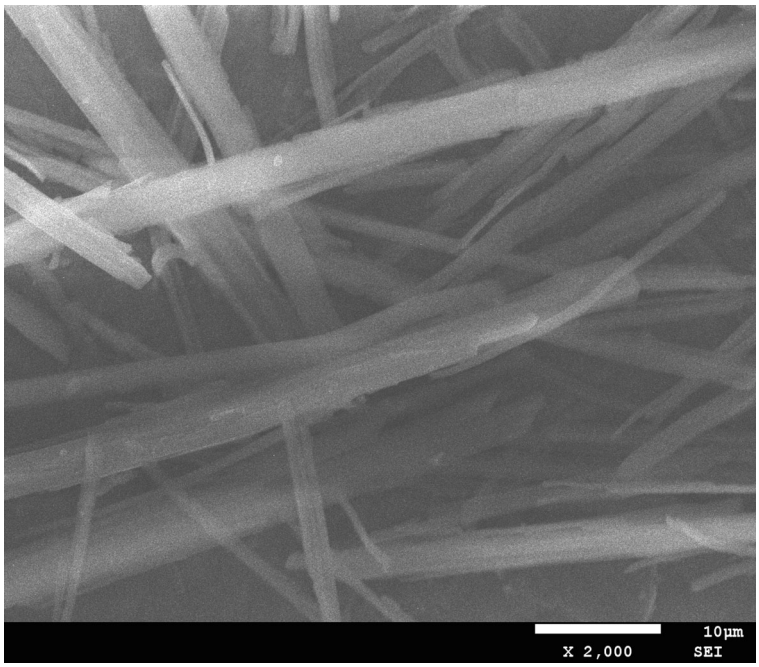

Fig. 2 SEM images of Zn-salen

interactions (Pinholt et al. 2013), Zn-salen adsorbs cationic dyes better than the anionic dyes. These results show that adsorption of substrate by Zn-salen is controlled mainly by surface charge interactions, which in turn will lead to the selective degradation of electropositive substrates.

3.3 Photocatalytic Degradation of Dyes and Colorless Organic Molecules by Zn-Salen

The photocatalytic degradation rates of RhB, SRB, MB, and Org II with Zn-salen under visible light irradiation at pH = 6.8 were measured to characterize the photocatalytic activity of Zn-salen (Fig. 3). MB (97.9 % after 180 min) exhibits the highest degradation rate, and RhB was also effectively degraded (97.1 % after 240 min) over Zn-salen. This is consistent with the observed degree of adsorption by Zn-salen. Neither SRB nor Org II shows an appreciable degradation over 4 h of light irradiation compared to MB and RhB which is attributed to their weaken adsorptions on Zn-salen. The results indicate the selective adsorption and subsequent photodegradation of target pollutants by Zn-salen.

To further understand the selectivity of the catalyst, zeta potential of the catalyst was measured. As can be seen from the online resource (Fig. S2), the point of zero charge (pzc) occurs at pH 4.75, indicating that the catalyst possesses a negative surface

Table 2 The adsorption data of dyes with Zn-salen ([Zn-salen] = 0.1 g/L; pH = 6.8)

	Q_{max} (mg/g)	k	R^2
RhB	0.023	$2.01*10^3$	0.998
MB	0.025	$1.13*10^3$	0.993
Org II	0.004	$6.78*10^2$	0.965
SRB	0.002	$3.46*10^2$	0.984

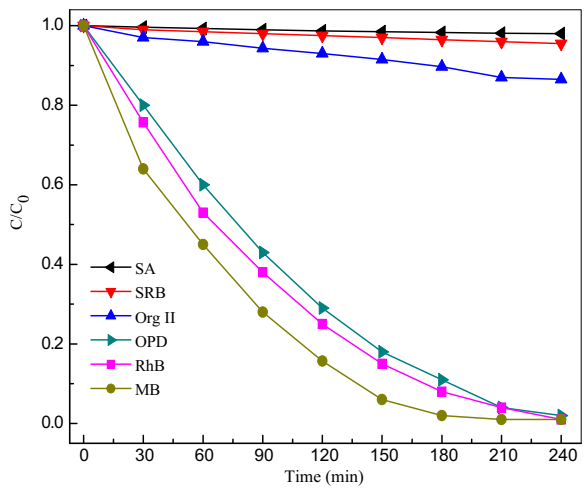

Fig. 3 Photocatalytic degradation of organic substrates over Zn-salen [Zn-salen] = 0.1 g/L; initial concentration $C_0 = 1.0 \times 10^{-5}$ mol/L; pH = 6.8

charge at higher pH values. As depicted in Table 2, cationic pollutants are selectively adsorbed over the catalyst surface, suggesting that columbic interactions are crucial in the adsorption process. Subsequently, surface adsorbed pollutants are preferentially degraded by photogenerated ROS (Fig. 3). Generally, the observed selectivity is mainly due to the adsorption pattern which is attributed to the charge interactions which allow pollutants to be in close vicinity with surface-generated ROS during light irradiation leading to selective photocatalytic degradation.

The photocatalytic degradation of colorless small molecules was also used to evaluate the characteristics and efficiency of a catalytic system (Wang et al. 2011). Moreover, to confirm the selective degradation of electropositive organic pollutants by Zn-salen, the degradation of SA and OPD, which do not absorb light in the visible region, were investigated under the same conditions (Fig. 3). The degradation result of OPD (96.5 % after 240 min) was similar to that obtained for MB and RhB, suggesting that the photocatalytic system is efficient in selectively degrading electropositive organic pollutants by photoexcitation of Zn-salen not photosensitization of substrates.

To further understand the selectivity of the catalyst, photocatalytic degradation of RhB in the presence of two surfactants was compared (Fig. 4). The addition of CTAB, a well-known cationic surfactant, inhibited RhB degradation ($K = 0.0014\ min^{-1}$), while SRB degradation was enhanced ($K = 0.0137\ min^{-1}$). The positive charge on quaternary ammonium of CTAB will interact with the negative charge of the sulfonyl group in SRB, exposing the positive charge of amino nitrogen in SRB molecule. Meanwhile, the addition of SDS, a well-known anionic surfactant, shows no significant effect on the degradation of RhB. These results imply that the electronegativity of the Zn-salen catalyst leads to selective adsorption and photocatalytic activity.

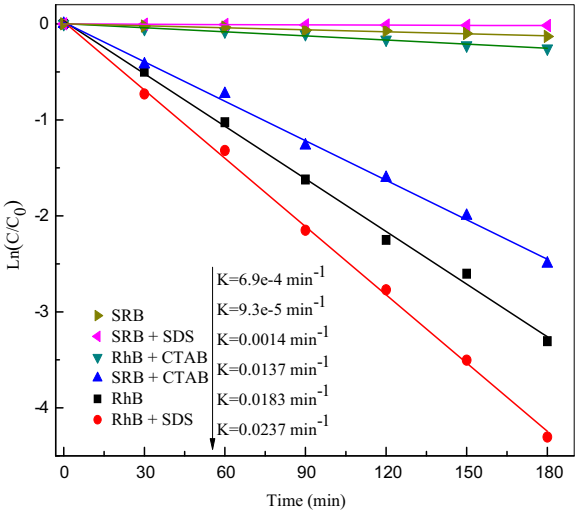

Fig. 4 Kinetic study for the effect of surfactant on the photocatalytic degradation of RhB over Zn-salen. [CTAB] = 0.2 g/L; [SDS] = 0.2 g/L; [Zn-salen] = 0.1 g/L; initial concentration of RhB $C_0 = 1.0 \times 10^{-5}$ mol/L; pH = 6.8

3.4 Effect of pH

The pH of the solution significantly affects the photocatalytic degradation of pollutants by changing the surface charge of the photocatalyst and substrate. To examine the effect of pH, photocatalytic degradation of RhB by Zn-salen was conducted at pH values of 3.05, 4.95, 6.88, 8.95, and 11.10. The results presented in Fig. 5 show that the pH has a significant effect on the degradation. Degradation rates of RhB increase with increasing pH from 3.05 to 11.10. The degradation of RhB is suppressed under acid conditions. Moreover, as can be seen from the online resource (Fig. S2), the zeta potential of Zn-salen varies with pH. The pzc occurs at pH = 4.75, indicating that the catalyst surface is negatively charged in neutral solution and the selectivity of the catalyst towards cationic substrates can be attributed to the electrostatic interactions that result in selective adsorption.

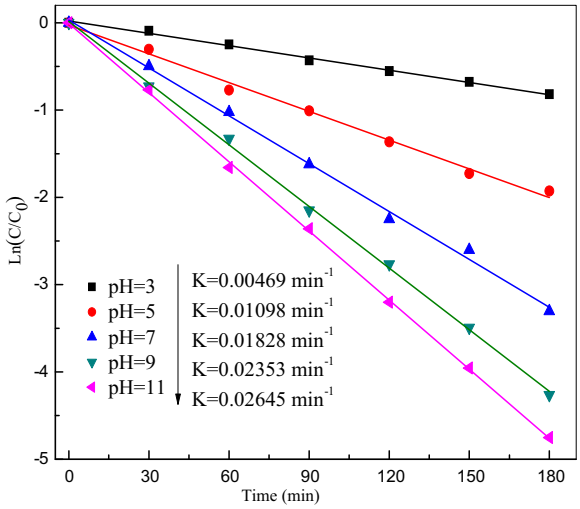

Fig. 5 Effect of pH on the photocatalytic degradation of RhB

3.5 IR Spectra Analysis of Intermediate in Photocatalytic Degradation of RhB

Changes in the structure of RhB caused by photocatalytic degradation were monitored by FT-IR spectroscopy, and the results are displayed in the online resource (Fig. S3). The characteristic absorption bands at 1340, 1180, and 1079 cm^{-1}, representing the methyl group ν(C–CH_3), aryl nitrogen ν(Ar–N), and ether linkage ν(–C–O–C–), respectively, are not present in the spectra of degradation products after 3, 9, and 15 h, which indicated that the primary groups, like (NEt_2) and (–C–O–C–), were decomposed during degradation. The new bands at 1630 and 1120 cm^{-1}, attributed to δ(NH_2) and ν(C–N), respectively, appeared in the spectra of products at 3, 9, and 15 h. It can be concluded that Ar–N and –C–O–C– in the RhB molecule are converted to primary amines, water, and carbon dioxide in the process of photocatalytic degradation.

3.6 Effect of Wavelength on the Photocatalytic Degradation

The response of Zn-salen to light was investigated by comparing the degradation rate of RhB over Zn-salen under different irradiation wavelengths (Fig. 6). No significant degradation occurs in the dark with the catalyst, indicating that light is necessary for the formation

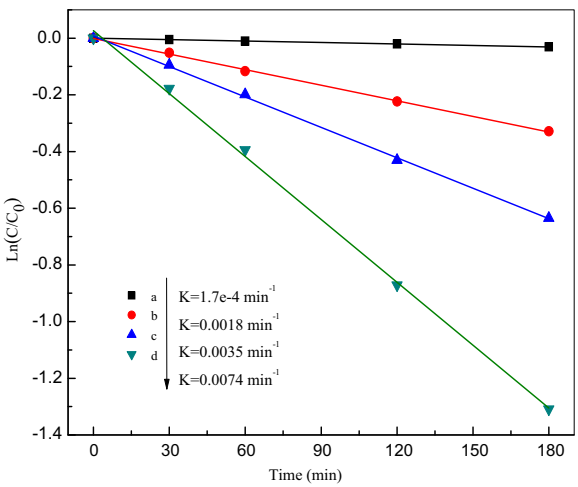

Fig. 6 Effect of wavelength on photocatalytic degradation of RhB over Zn-salen in the dark (*a*) and at $\lambda = 450$ nm (*b*), $\lambda = 365$ nm (*c*), and $\lambda = 420$ nm (*d*). [Zn-salen] = 0.1 g/L; initial concentration of RhB $C_0 = 1.5 \times 10^{-5}$ mol/L; pH = 6.8

of ROS. The extent of RhB degradation was the highest (97.9 % after 300 min) under visible light irradiation at 420 nm. In contrast, the percentage of RhB degradation decreases when irradiated with light with a wavelength of 365 or 450 nm (42.8 and 73.4 %, respectively, after 300 min).

Based on the observed results, we postulate that light-activated Zn-salen undergoes a series of energy transfer and electron transfer reactions that generate singlet oxygen ($^1O_2$) and superoxide ion radical ($O_2\cdot^-$). The ESR technology is an effective method to monitor the existence of these short-lived radicals. Figure 7 shows the characteristic signals of TEMP-$^1O_2$ adducts (A) and DMPO-$O_2^{\cdot-}$ adducts (B) at different times. It can be seen that characteristic triplet peaks of TEMP-$^1O_2$ adducts with an intensity ratio of 1:1:1 were detected during visible light irradiation and dark reaction condition, indicating that $^1O_2$ is not the main reactive oxygen species generated by the photoexcitation of Zn-salen. The ESR signals of DMPO-$O_2\cdot^-$ adduct were also observed in the system under visible light irradiation only. It suggests that the catalytic mechanism mainly involves the $O_2\cdot^-$ oxidation mechanism. The same results were detected in the degradation of both SRB and RhB by Zn-salen in the presence of CTAB. It indicates that the surfactant has no effect on the generation of reactive oxygen species.

Appropriate scavengers for $^1O_2$, $O_2\cdot^-$, and ·OH (hydroxyl radical) were used to identify the ROS involved in the photodegradation of RhB over Zn-salen, and the results are presented in the online resource (Fig. S4). The addition of *tert*-butanol, a well-known ·OH quencher, showed no significant effect on degradation of RhB. The addition of sodium azide (NaN_3), an $^1O_2$ quencher, slightly decreases the degradation rate of RhB. Moreover, the addition of *p*-benzoquinone, an $O_2\cdot^-$ quencher, clearly suppresses the degradation of RhB (Fig. S4). This demonstrates that both $^1O_2$ and $O_2\cdot^-$ are involved in the photocatalytic degradation, but $O_2\cdot^-$ appears to be the primary ROS.

To further understand the photocatalytic mechanism, the catalyst bandgap was estimated from a plot of the transformed Kubelka–Munk function versus the energy of absorbed light (Fig. 1). The optical bandgap is calculated to be 2.4 eV. The conduction band (CB) edge position of a semiconductor at the point of zero charge was evaluated at −0.78 eV when using the empirical formula expressed by

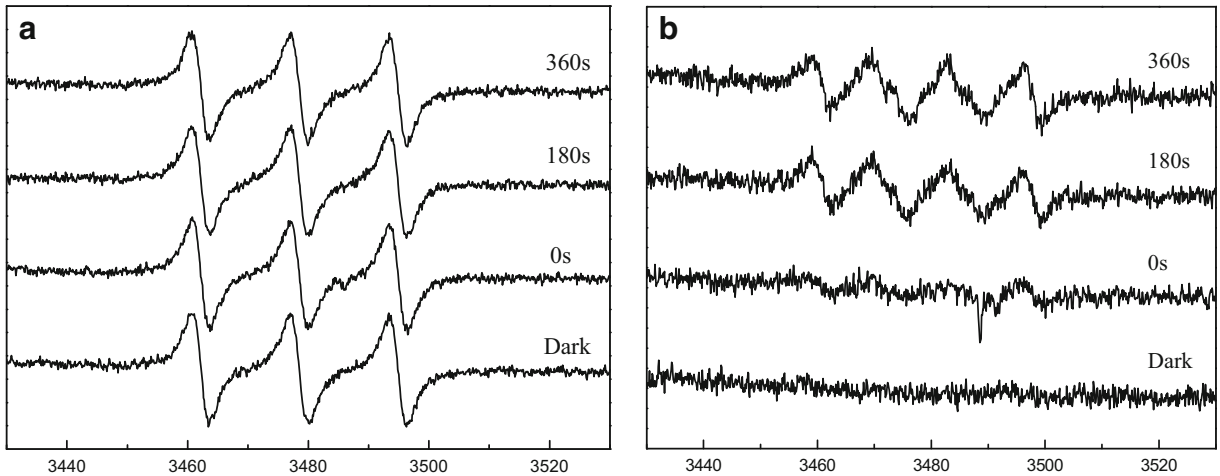

Fig. 7 ESR signals of the TEMP-$^1O_2$ adducts (A) and DMPO-$O_2{\cdot}^-$ adducts (B)

$E_{CB} = X - E^e - 0.5E_g$, where E_{CB} was the CB edge potential, X is the geometric mean of the electronegativity of the constituent atoms, E^e is the energy of free electrons on the hydrogen scale (≈4.5 eV), and E_g is the bandgap energy of the semiconductor. Correspondingly, the valence band potential was calculated at about 1.62 eV.

Under visible light irradiation, the Zn-salen can adsorb incident photons leading to the formation of charge carriers. Then, the photogenerated electrons and positive holes migrate to the surface of the Zn-salen and participate in the redox reaction. Since the conduction band of Zn-salen (−0.78 V vs. normal hydrogen electrode (NHE)) is more negative than the redox potential of O_2/O_2^- (−0.33 V vs. NHE), it is energetically permissible for the photogenerated electron to transfer from the catalyst to the adsorbed molecular oxygen. In contrast, the valence band (VB) of Zn-salen (1.62 V vs. NHE) is higher than the redox potential of ·OH/OH− (2.38 V vs. NHE) which makes the formation of hydroxyl radical difficult. On the contrary, the redox potential of dyes such as RhB and MB is significantly lower than the VB level of Zn-salen, suggesting that direct hole oxidation of pollutants is also energetically favorable. This is in agreement with the observed results in quenching and ESR experiments.

Based on the above results, Eqs. 2 to 9 present the general mechanism for the photoexcitation and electron transfer properties of the Zn-salen for the photocatalytic degradation of pollutants under visible light irradiation (Marais et al. 2007; Zhang et al. 2013).

$$\text{Zn-salen} + h\nu \rightarrow {}^1\text{Zn-salen}^* \rightarrow {}^3\text{Zn-salen}^* \quad (2)$$

$${}^3\text{Zn-salen}^* + O_2 \rightarrow \text{Zn-salen}^{\cdot+} + O_2{\cdot}^- \quad (3)$$

$${}^3\text{Zn-salen}^* + {}^3O_2 \rightarrow \text{Zn-salen} + {}^1O_2 \quad (4)$$

$${}^3\text{Zn-salen}^* + \text{Subs} \rightarrow \text{Zn-salen}^{\cdot-} + \text{Subs}^{\cdot+} \quad (5)$$

$$\text{Zn-salen}^{\cdot-} + O_2 \rightarrow \text{Zn-salen} + O_2{\cdot}^- \quad (6)$$

$$\text{Zn-salen}^{\cdot-} + \text{Zn-salen}^{\cdot+} \rightarrow 2\text{Zn-salen} \quad (7)$$

$$O_2{\cdot}^- + \text{Subs} \rightarrow \text{oxidation products} \quad (8)$$

$${}^1O_2 + \text{Subs} \rightarrow \text{oxidation products} \quad (9)$$

Light-activated Zn-salen leads to the formation of the singlet state (^{1}Zn-salen*) which then relaxes to the triplet state (^{3}Zn-salen*). The ^{3}Zn-salen* interacts with ground-state molecular oxygen generating $O_2{\cdot}^-$ and $^1O_2$, which subsequently degrades the substrate. Moreover, the absence of O_2 restrains the degradation process based on the cyclic reaction (Fig. S4).

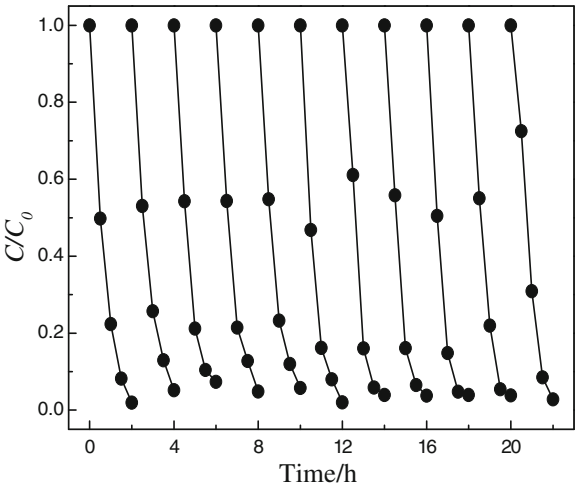

Fig. 8 Repeated cycles of RhB photocatalytic degradation over Zn-salen [Zn-salen] = 0.1 g/L; $[RhB]_0 = 1.0 \times 10^{-5}$ mol/L; pH = 6.8

3.7 Stability and Reusability of the Zn-Salen Photocatalyst

The stability of heterogeneous photocatalysts such as Zn-salen is important in the treatment of water and wastewater. To test the stability of the Zn-salen catalyst, photocatalytic degradation of RhB was repeated 11 times with the same catalyst. After each run, the solution residue was filtered, washed and dried, and used again under identical conditions. The degradation data (Fig. 8) confirm that the catalytic activity of Zn-salen was maintained after recycling the catalyst 11 times; degradation ratios remained near 95 %. The Zn-salen catalyst is an effective and stable catalyst, activated by visible light with good potential for application in the degradation of organic pollutants in water.

4 Conclusions

In summary, this study demonstrates a promising approach for the activation of molecular oxygen by a newly developed heterogeneous photocatalyst. Water-insoluble Schiff base complex (Zn-salen) with strong visible light absorption was employed successfully as a heterogeneous photocatalyst to degrade organic pollutants in aqueous solution at a wide range of pH (>3). Zn-salen displays selective adsorption and degradation of electropositive organic substrates due to its electronegative surface. Under visible light irradiation, Zn-salen interacts with O_2 to produce $O_2^{\cdot -}$ and $^1O_2$ and can abstract electrons from the substrate. Zn-salen demonstrates high stability, selectivity, recyclability, and the ability to work over a wide range of pH.

Acknowledgments This work was funded by the National Natural Science Foundation of China (Nos. 21407092, 21377067, and 21577077) and the Natural Science Foundation for Innovation Group of Hubei Province, China (No. 2015CFA021).

References

Ahmed, B., Limem, E., Abdel-Wahab, A., & Nasr, B. (2011). Photo-Fenton treatment of actual agro-industrial wastewaters. *Ind Eng Chem Res., 50*, 6673–6680.

Ali, M. M., & Sandhya, K. Y. (2016). Selective photodegradation and enhanced photo electrochemical properties of titanium dioxide–graphene composite with exposed (001) facets made by photochemical method. *Sol Energ Mat Sol C., 144*, 748–757.

Ardo, S., Achey, D., Morris, A. J., Abrahamsson, M., & Meyer, G. J. (2011). Non-Nernstian two-electron transfer photocatalysis at metalloporphyrin–TiO_2 interfaces. *J Am Chem Soc., 133*, 16572–16580.

Boukha, Z., González-Prior, J., Rivas, B. D., González-Velasco, J. R., López-Fonseca, R., & Gutiérrez-Ortiz, J. I. (2016). Synthesis, characterization and behavior of Co/hydroxyapatite catalysts in the oxidation of 1,2-dichloroethane. *Applied Catalysis B: Environmental, 190*, 125–136.

Bozell, J. J., Hames, B. R., & Dimmel, D. R. (1995). Cobalt-Schiff base complex catalyzed oxidation of para-substituted phenolics. Preparation of benzoquinones. *J. Org. Chem., 60*, 2398–2404.

Buddhadeb, D., Sreyashi, J., Rajesh B., Pratap., Kumar, S., Subratanath K. (2007). Immobilization of copper Schiff base complexes in zeolite matrix: preparation, characterization and catalytic study. Applied Catalysis A: General, 318, 89–94

Chen, X., Ma, W. H., Li, J., Wang, Z. H., Chen, C. C., Ji, H. W., & Zhao, J. C. (2011a). Photocatalytic oxidation of organic pollutants catalyzed by an iron complex at biocompatible pH values: using O_2 as main oxidant in a Fenton-like reaction. *J Phys Chem C., 115*, 4089–4095.

Chen, L. W., Ma, J., Li, X. C., Zhang, J., Fang, J. Y., Guan, Y. H., & Xie, P. C. (2011b). Strong enhancement on Fenton oxidation by addition of hydroxylamine to accelerate the ferric and ferrous iron cycles. *Environ Sci Technol., 45*, 3925–3930.

Chen, Y., Zhang, K., & Zuo, Y. (2013). Direct and indirect photodegradation of estriol in the presence of humic acid, nitrate and iron complexes in water solutions. *Science of the Total Environment, 463–464*, 802–809.

Claudio, P., Fabio, M., Riccardo, P., Domenico, M., Andrei, D., & Sergei, T. (2001). Synthesis and characterisation of tin(IV) and organotin(IV) derivatives 2-{[(2-hydroxyphenyl) imino] methyl} phenol. *Inorg Chim Acta., 325*, 103–114.

Cotanda, P., Lu, A., Patterson, J. P., Petzetakis, N., & O'Reilly, R. K. (2012). Functionalized organocatalytic nanoreactors:

hydrophobic pockets for acylation reactions in water. *Macromolecules, 45*, 2377–2384.

Drozd, D., Szczubiałka, K., Łapok, Ł., Skiba, M., Patel, H., Gorun, S. M., & Nowakowska, M. (2012). Visible light induced photosensitized degradation of acid orange 7 in the suspension of bentonite intercalated with perfluoroalkyl perfluoro phthalocyanine zinc complex. *Appl Catal B: Environ., 125*, 35–40.

El-Medani, S. M., Ali, O. A. M., & Ramadan, R. M. (2005). Photochemical reactions of group 6 metal carbonyls with N-salicylidene-2-hydroxyaniline and bis-(salicylaldehyde) phenylenediimine. *J Mol Struct., 738*, 171–177.

Fang, Y. F., Huang, Y. P., Yang, J., Wang, P., & Cheng, G. W. (2011). Unique ability of BiOBr to decarboxylate D-Glu and D-MeAsp in the photocatalytic degradation of microcystin-LR in water. *Environ Sci Technol., 45*, 1593–1600.

Fatemeh, S. S., & Kamran, A. (2016). Linkers and coordinated solvent molecules; the two effective factors on formation of zinc oxide nanoparticles from metal–organic frameworks. *Inorg Chem Commun., 63*, 5–10.

Gonzalez-Olmos, R., Martin, M. J., Georgi, A., Kopinke, F. D., Oller, I., & Malato, S. (2012). Fe-zeolites as heterogeneous catalysts in solar Fenton-like reactions at neutral pH. *Appl Catal B: Environ., 125*, 51–58.

Gupta, K. C., Kumar, S. A., & Lin, C. C. (2009). Polymer-supported Schiff base complexes in oxidation reactions. *Coord Chem Rev., 253*, 1926–1946.

Hu, X. B., Xu, X., Ji, F. Y., & Fan, Z. H. (2009). Preparation and catalytic kinetic of hydrophobic photocatalytic catalysts. *J Inorg Mater., 24*, 1115–1120.

Huang, Y. P., Li, J., Ma, W. H., Cheng, M. M., Zhao, J. C., & Yu, J. C. (2004). Efficient H_2O_2 oxidation of organic pollutants catalyzed by supported iron sulfophenylporphyrin under visible light irradiation. *J Phys Chem B., 108*, 7263–7270.

Huang, Y. P., Ma, W. H., Li, J., Cheng, M. M., Zhao, J. C., Wan, L. J., & Yu, J. C. (2003). A novel β-CD-hemin complex photocatalyst for efficient degradation of organic pollutants at neutral pHs under visible irradiation. *J Phys Chem B., 107*, 9409–9414.

Kubacka, A., Fernández-García, M., & Colón, G. (2012). Advanced nanoarchitectures for solar photocatalytic applications. *Chem Rev., 112*, 1555–1614.

Liu, L., Jiang, D. L., McDonald, A., Hao, Y. Q., Millhauser, G. L., & Zhou, F. M. (2011). Copper redox cycling in the prion protein depends critically on binding mode. *J Am Chem Soc., 133*, 12229–12237.

Liu, S., Peng, J. J., Yang, H., Bai, Y., Li, J. Y., & Lai, G. Q. (2012). Highly efficient and convenient asymmetric hydrosilylation of ketones catalyzed with zinc Schiff base complexes. *Tetrahedron Lett., 68*, 1371–1375.

Mahamuni, N. N., & Adewuyi, Y. G. (2010). Advanced oxidation processes (AOPs) involving ultrasound for waste water treatment: a review with emphasis on cost estimation. *Ultrason Sonochem., 17*, 990–1003.

Marais, E., Klein, R., Antunes, E., & Nyokong, T. (2007). Photocatalysis of 4-nitrophenol using zinc phthalocyanine complexes. *J Mol Catal A: Chem., 261*, 36–42.

Meng, X., Qin, C., Wang, X. L., Su, Z. M., Li, B., & Yang, Q. H. (2011). Chiral salen-metal derivatives of polyoxometalates with asymmetric catalytic and photocatalytic activities. *Dalton T., 40*, 9964–9966.

Niu, P., Yang, Y., Yu, J. C., Liu, G., & Cheng, H. (2014). Switching the selectivity of the photoreduction reaction of carbon dioxide by controlling the band structure of a g-C_3N_4 photocatalyst. *Chem. Commun, 50*, 10837–10840.

O'Shea, K. E., & Dionysiou, D. D. (2012). Advanced oxidation processes for water treatment. *J Phys Chem Lett., 3*, 2112–2113.

Pinholt, C., Kapp, S. J., Bukrinsky, J. T., Hostrup, S., Frokjaer, S., Norde, W., & Jorgensen, L. (2013). Influence of acylation on the adsorption of GLP-2 to hydrophobic surfaces. *Int J Pharm., 440*, 63–71.

Qianqian, Z., Mami, I., Masahide, S., Takafumi, M., Ritsu, K., & Masami, F. (2016). Degradation and debromination of bromophenols using a free-base porphyrin and metalloporphyrins as photosensitizers under conditions of visible light irradiation in the absence and presence of humic substances. *Appl Catal B: Environ., 183*, 61–68.

Ryo, N., Shin-ichi, N., & Hiroaki, T. (2015). Visible light-driven selective aerobic oxidation of benzylalcohols to benzaldehydes by a $Cu(acac)_2$–$BiVO_4$-admicelle three-component heterosupramolecular photocatalyst. *J Phys Chem C., 119*, 11771–11776.

Sharma, R. K., Gulati, S., Pandey, A., & Adholeya, A. (2012). Novel, efficient and recyclable silica based organic–inorganic hybrid nickel catalyst for degradation of dye pollutants in a newly designed chemical reactor. *Appl Catal B: Environ., 125*, 247–258.

Silva, M., Calvete, M. J. F., Gonçalves, N. P. F., Burrows, H. D., Sarakha, M., Fernandes, A., Ribeiro, M. F., Azenha, M. E., & Pereira, M. M. (2012). Zinc(II) phthalocyanines immobilized in mesoporous silica Al-MCM-41 and their applications in photocatalytic degradation of pesticides. *J Hazard Mater., 233*, 79–88.

Sofianou, M. V., Psycharis, V., Boukos, N., Vaimakis, T., Yu, J., Dillertd, R., Bahnemann, D., & Christos, T. (2013). Tuning the photocatalytic selectivity of TiO_2 anatase nanoplates by altering the exposed crystal facets content. *Applied Catalysis B: Environmental, 142–143*, 761–768.

Song, Q., Jia, M. K., Ma, W. H., Fang, Y. F., & Huang, Y. P. (2013). Heterogeneous degradation of toxic organic pollutants by hydrophobic copper-Schiff base complex under visible irradiation. *Sci China Chem., 56*, 1–8.

Song, Q., Ma, W. H., Jia, M. K., David, J., & Huang, Y. P. (2015). Degradation of organic pollutants in waters by a water-insoluble iron(III) Schiff base complex. *Appl Catal A Gen., 505*, 70–76.

Su, R., Sun, J., Sun, Y. P., Deng, K. J., Cha, D. M., & Wang, D. Y. (2009). Oxidative degradation of dye pollutants over a broad pH range using hydrogen peroxide catalyzed by $FePz(dtnCl_2)_4$. *Chemosphere., 77*, 1146–1151.

Tianyuan, X., Yun, L., Fei, G., Lin, L., & Yuting, O. (2013). Application of response surface methodology for optimization of azocarmine B removal by heterogeneous photo-Fenton process using hydroxy-iron–aluminum pillared bentonite. *Appl Surf Sci., 280*, 926–932.

Tseng, W. J., & Lin, R. D. (2014). $BiFeO_3$/α-Fe_2O_3 core/shell composite particles for fast and selective removal of methyl orange dye in water. *Journal of Colloid and Interface Science, 428*, 95–100.

Vijayaraj, A., Prabu, R., Suresh, R., Sivaraj, C., Raaman, N., & Narayanan, V. (2011). New a cyclic Schiff-base copper(II)

complexes and their electrochemical, catalytic, and antimicrobial studies. *J Coord Chem., 64*, 637–650.

Wang, X. L., Chen, N. L., Liu, G. C., Tian, A. X., Sha, X. T., & Ma, K. F. (2015). A series of Cd^{II}/Zn^{II} coordination polymers containing helical chains constructed from a "V"-like bis-pyridyl-bis-amide and various dicarboxylates: assembly, structures, photoluminescent and selective photocatalysis. *Inorg. Chim. Acta., 432*, 128–135.

Wang, S. L., Fang, Y. F., Yang, Y., Liu, J. Z., Deng, A. P., Zhao, X. R., & Huang, Y. P. (2011). Catalysis of organic pollutant photodegradation by metal phthalocyanines immobilized on TiO_2@SiO_2. *Chin Sci Bull., 56*, 969–976.

Warren, J. E., Perkins, C. G., Jelfs, K. E., Boldrin, P., Chater, P. A., Miller, G. J., Manning, T. D., Briggs, M. E., Stylianou, K. C., Claridge, J. B., & Rosseinsky, M. J. (2014). Shape selectivity by guest-driven restructuring of a porous material. *Angew. Chem. Int. Edn., 53*, 4592–4596.

Wu, Q., Lin, S. W., Li, Y. G., & Wang, E. B. (2012). New supramolecular hybrids based on A-type Anderson polyoxometalates and Mn–Schiff-base complexes. *Inorg Chim Acta., 382*, 139–145.

Xiaopeng, W., Shouqiang, H., Nanwen, Z., Ziyang, L., & Haiping, Y. (2015). Facile synthesis of porous TiO_2 photocatalysts using waste sludge as the template. *Appl Surf Sci., 359*, 917–922.

Ye, L., Yang, C., Tian, L., Zan, L., & Peng, T. (2011). Tunable photocatalytic selectivity of fluoropolymer PVDF modified TiO_2. *Appl Surf Sci., 257*, 8072–8077.

Zhang, Z. H., Zhang, M. J., Deng, J., Deng, K. J., Zhang, B. G., Lv, K. L., Sun, J., & Chen, L. Q. (2013). Potocatalytic oxidative degradation of organic pollutant with molecular oxygen activated by a novel biomimetic catalyst ZnPz(dtn-$COOH)_4$. *Appl Catal B: Environ., 132*, 90–97.

Zhao, X., Bu, X., Wu, T., Zheng, S., Wang, L., & Feng, P. (2013). Selective anion exchange with nanogated isoreticular positive metal-organic frameworks. *Nature communications, 4*, 2344.

Zhao, X. G., Huang, J. G., Wang, B., Bi, Q., Dong, L. L., & Liu, X. J. (2014). Preparation of titanium peroxide and its selective adsorption property on cationic dyes. *Appl Surf Sci., 292*, 576–582.

Zou, C., Zhang, Z. J., Xu, X., Gong, Q. H., Li, J., & Wu, C. D. (2012). A multifunctional organic–inorganic hybrid structure based on Mn^{III}–porphyrin and polyoxometalate as a highly effective dye scavenger and heterogenous catalyst. *J Am Chem Soc., 134*, 87–90.

Zuo, Y., & Deng, Y. (1997). Iron (II) catalyzed photochemical decomposition of oxalic acid and generation of H_2O_2 in atmospheric liquid phases. *Chemosphere, 35*, 2051–2058.